Supported iridium catalysts for the total oxidation of short chain alkanes and their mixtures: influence of the support

Lukas Schick [a,b], Vicenta González-Alfaro [a], Adrián García [a], J.M. López [c], David J. Morgan [d], Said Agouram,[e] Stuart H. Taylor[d,*], Tomás García[c,*] and Benjamin Solsona[a,*]

[a] Departament d'Enginyeria Química, ETSE, Universitat de València, Av. Universitat, 46100, Burjassot-Valencia, Spain.

[b] Accumulators Materials Research, Center for Solar Energy and Hydrogen Research Baden-Württemberg (ZSW), 89073 Ulm, Germany.

[c] Instituto de Carboquímica (CSIC), C/Miguel Luesma 4, 50018 Zaragoza, Spain.

[d] Cardiff Catalysis Institute, School of Chemistry, Cardiff University, Main Building, Park place, Cardiff, CF10 3AT, UK.

[e] Department of Applied Physics and Electromagnetism, Universitat de València, 46100 Burjassot-Valencia, Spain.

[*] Corresponding authors.

E-mail addresses: taylorsh@cardiff.ac.uk (S.H. Taylor), tomas@icb.csic.es (T. García), Benjamin.solsona@uv.es (B. Solsona)

Abstract

Catalytic total oxidation of noxious volatile organic compounds (VOCs) is an important process to remove these compounds from the atmosphere. This is the first systematic study of the influence of the support on the activity of iridium oxide supported catalysts for the total oxidation of VOCs. Iridium catalysts supported on titania, γ-alumina, silica and zeolites have been prepared using different calcination temperatures. The activity for the total oxidation of short chain alkanes and their mixtures has been evaluated and the physicochemical properties characterized by N_2 adsorption, XRD, (HR)TEM, EDX, CO-Chemisorption, TPR, XPS and Raman spectroscopy. Both the calcination temperature and the nature of the support of iridium catalysts play an important role for the catalytic performance. Silica, ZSM-5 zeolites and titania are suitable supports for IrOx, in contrast with γ-alumina. A strong influence of the Lewis acidity of the support on the turnover frequency of the iridium oxide is found. Additionally, for a given support, the calcination temperature has an effect on the catalytic activity. A possible size effect is discussed. However, the major controlling factor is the nature of the support. Therefore, our results provide a guideline towards a rational design of more active IrOx catalysts for the total oxidation of VOCs.

Introduction

It is widely known that volatile organic compounds (VOCs) are linked to the formation of ground level ozone and fine particulates, forming urban smog. Therefore, VOCs contribute to health problems like heart disease and asthma [1], as well as the fact that some of them are intrinsically toxic and carcinogenic [2]. The definition of VOCs is broad and includes chemically diverse carbon compounds with a high vapour pressure under standard conditions, which participate in atmospheric photochemical reactions [3]. The main anthropogenic sources of VOCs include combustion processes, chemical and pharmaceutical plants, power generation, gas stations and textile manufacturing [3]. Due to their toxicity and health risks, various methods for VOC abatement have been developed [4]. These include adsorption, absorption, condensation, thermal oxidation and catalytic oxidation. Total oxidation using a heterogeneous catalyst is very effective for the removal of low concentrations of VOCs and requires less energy in the form of heating compared to thermal oxidation. Therefore, catalytic total oxidation is an important process for the removal of VOCs [3].

Most active catalysts for total oxidation of VOCs are based on noble metals, such as gold, platinum and palladium, which present the drawback of their relatively high prices. Iridium is about 15% cheaper than gold and 30% cheaper than palladium, although it remains more expensive than platinum (1st September 2020) [https://www.metalsdaily.com/live-prices/pgms/].

However, there are very few articles dedicated to the study of iridium catalysts for the removal of pollutants [5]. In the case of the total oxidation of volatile organic compounds, iridium catalysts potentially have high activity [6]–[8]. In a previous study focused on silica supported iridium oxides, we reported the high activity of these

catalysts for the total oxidation of short chain alkanes, surpassing the performance of similar Pd and Au catalysts. Additionally, we reported that lower calcination temperatures resulted in more reduced iridium oxide species and small particles with higher activity for the total oxidation of short chain alkanes [9].

For CO oxidation, highly dispersed single-atom iridium species deposited on $MgAl_2O_4$ have shown notable catalytic properties due to the formation of highly active Ir(CO) species, which can easily activate O_2 molecules [10]. In the water gas shift reaction iridium on iron oxide has been shown to be even more reactive than catalysts containing Au or Pt. The high activity has been related to the formation of reactive vacancies in the iron oxide matrix, consequently improving its reducibility [11]. It should also be mentioned that Ir-based catalysts have shown good efficiency for other reactions, such as hydrogenation, ring-opening, isomerization and alkylation [12–15].

The use of iridium in multicomponent catalysts with other metals, such as platinum [16–18] or nickel [19], has also led to enhanced catalytic performance. In the total oxidation of methane using zirconium oxide as a support, catalysts based on iridium were highly active, but less active than those with Pd or Pt [6]. Interestingly, the addition of Ir to Pt resulted in the highest catalytic activity and lower deactivation in the presence of sulphur. The stabilizing effect of iridium on the catalytic activity in the presence of SO_2 was associated with the stabilization of platinum as a highly oxidized species (Pt^{4+}). This stabilization of Pt as an oxidized species prevents the SO_2-induced reduction of platinum, which is accompanied by a stabilization of the catalytic activity. In other work, TiO_2 supported Pt, Pd, Ir, Rh and Au catalysts were evaluated for the total oxidation of CO and two representative VOCs [7]. For the oxidation of VOCs, the Pt catalyst was the most active, whereas the Au catalyst was the least active and the Ir catalyst showed intermediate performance. In the case of Pt and Pd catalysts it was

observed that the oxidation of toluene and ethanol were structure sensitive reactions, whereas insufficient catalysts containing iridium were studied in order to conclude whether a possible structure-activity relationship existed. The total oxidation of alkanes on Pt and Pd based catalysts follows a Mars-Van-Krevelen mechanism [3]. A schematic illustration and a short description of the reported reaction pathway are presented in Scheme S1 of the Supporting Information.

Iridium itself can either be present as a metal in reducing environments or as an oxide in oxidizing environments. Pure Iridium oxidizes in air above 600°C to IrO_2 [20]. IrO_2 has a Rutile structure, space group P42/mnm (136) with lattice parameters a = b = 4.499 Å and c = 3.154 Å [21]. Utilizing experimental results and DFT calculations, He *et al.* showed that a hexagonal multilayer oxide with a corundum Ir_2O_3 structure (a = b = 5.168 Å and c = 12.78 Å) is formed on Ir(111) surfaces at ~ 300°C and an oxygen partial pressure of 0.1 bar [22]. Ir_2O_3 is reported to be only kinetically stable [22] and formed via indirect pathways [20]. $Ir^{(III)}$ compounds are reported to be more stable in acidic environments, whereas $Ir^{(IV)}$ compounds are more stable in alkaline environments [23]. Ir_2O_3 decomposes around 400°C to form IrO_2 [20].

For supported noble metal catalysts, the nature of the support can affect the electronic structure i.e. the electron energy and electron density of the active metal atom. Supports with high Lewis acidity, such as TiO_2 and ZrO_2-SiO_2, draw electrons from the active metal, resulting in a $M^{\delta+}$ state of the active metal atoms [24]. Yazawa *et al.* argue that in oxidizing atmosphere the inductive effect of a Lewis acidic support increases the oxidation resistance of Pt. They list the acidic strength of the support in the order:

$$MgO < La_2O_3 < ZrO_2 < \mathbf{Al_2O_3} < \mathbf{SiO_2} < SiO_2\text{-}Al_2O_3 = SO_4{}^{2-}ZrO2$$
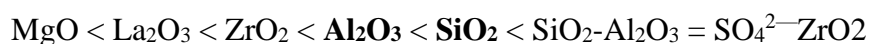
They found a correlation between the Lewis acid strength of the support and the oxidation state of the Pt catalyst. The Pt on the more acidic support is less oxidized (lower formal oxidation state of the Pt atoms) and offers higher catalytic activity for the total combustion of propane [25], [26]. In a publication by Nauert *et al.* the Lewis acidity is calculated for several oxide supports and follows the order [27]:

$$La_2O_3 < MgO < ZnO < \mathbf{Al_2O_3} < ZnO < \mathbf{TiO_2} < \mathbf{SiO_2} < Nb_2O_5 < Ta_2O_5$$
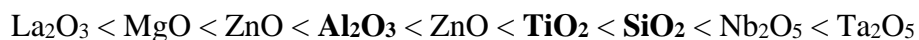
Additionally, the degree of interaction of the catalyst particles with the support depends on the particle size, as large particles interact less strongly with the support compared to smaller ones, facilitating substrate activation. The metal-support interaction also influences the catalytic activity in other reactions such as steam reforming and others [28-31]

Although there is no general consensus [32], [33], it has been reported that VOC total oxidation by platinum or palladium catalysts is a structure sensitive reaction, in which turnover rates increase when the particle size increases [34], [35]. Accordingly, the activity of large PdOx or PtOx crystallites is higher than those of small particles, due to increased efficacy for oxygen activation. For the readers convenience a short summary of possible origins of the reported structure sensitivity of PdOx and PtOx catalysts for the total oxidation of alkanes is presented in the Supporting Information.

In the present work, supported iridium oxide catalysts have been synthesized and applied for the total oxidation of propane, ethane and methane and their mixtures. Several calcination temperatures (350°C – 750°C) and different supports (titania, alumina, silica and ZSM-5 zeolites with different Si/Al ratios) have been evaluated. The physiochemical properties of the resulting catalysts are characterized thoroughly. The role of the support on the catalytic performance, as well as the way the support affects

the iridium species, has been studied. A particle size effect of the IrOx catalyst is discussed with respect to PtOx and PdOx catalysts.

Experimental

Catalyst preparation

The catalysts were synthesized using the incipient wetness impregnation method. The iridium salt employed was chloride-ion free $Ir(AcAc)_3$ (Sigma Aldrich, > 99%), which was dissolved in toluene (Sigma Aldrich > 99.8%). The utilization of the chloride-ion free $Ir(AcAc)_3$ salt eliminates the possibility of catalyst deactivation by chemisorption of chlorides. The amount of Ir was kept constant at 2 wt.% for all the catalysts tested. The amount of solvent required for incipient wetness was determined beforehand for all supports. Supports employed were SiO_2 (Degussa Aerosil 200, calcined at 800 °C for 2 h, $S_{BET} = 181$ m^2 g^{-1}), TiO_2 (Degussa P25, 90% Anatase 10% Rutile, $S_{BET} = 55$ m^2 g^{-1}) and γ-Al_2O_3 (Süd Chemie, $S_{BET} = 187$ m^2 g^{-1}). After impregnation the catalysts were dried at 55 °C for 6-10 hours, dried at 120 °C for 16 hours and finally calcined in air for two hours at temperatures between 350 and 750 °C.

Additionally, three ZSM-5 zeolites, with different SiO_2/Al_2O_3 ratios of 30 ($S_{BET} = 405$ m^2 g^{-1}), 50 ($S_{BET} = 425$ m^2 g^{-1}) and 80 ($S_{BET} = 425$ m^2 g^{-1}), supplied by Zeolyst, were used as supports. The Ir-catalysts present the same Ir-loading (2 wt.%) and were prepared in the same way as those with silica, alumina or titania. The calcination temperature was fixed at 550 ºC in air for two hours.

Characterization techniques

The specific surface area of the catalysts was determined from nitrogen adsorption desorption isotherms at -196 ºC. A Micromeritics ASAP-2020 automated analyzer was used. Prior to the analyses, the catalysts were degassed at 80 ºC for 5 h and 10^{-6} Torr. The Brunauer-Emmett-Teller (BET) model was used to calculate the surface areas.

The active IrOx surface area was determined with CO pulse chemisorption analyses using a Micromeritics Autochem 2920 instrument under cryogenic conditions, as used previously [36]. Catalysts were pre-reduced before the chemisorption experiments to have metallic Ir. For analysis of the results, a coordination of two CO molecules to an active iridium site is assumed.

Temperature programmed reduction (TPR) analyses have been performed in a Micromeritics Autochem 2920 instrument equipped with a thermal conductivity detector. The reduction step has been carried out in a 50 ml min^{-1} flow of 10% H_2/Ar between 40°C and 400°C with a heating rate of 20°C min^{-1}. These are standard conditions and are known to be within the kinetic regime.

The catalysts structure was characterized by powder X-ray diffraction (XRD) using a Bruker D8 Advance A25 diffractometer with monochromatic Cu$_{K\alpha1}$ radiation operated at 40 kV and 40 mA. Crystalline phases were identified by matching to diffraction data from the International Center for Diffraction Data for metallic Iridium (JCPDS 03-065-1686) and IrO$_2$ (JCPDS 00-043-1019). The crystalline structure of the corundum like Ir$_2$O$_3$ utilized for the Rietveld refinements is based on the lattice parameter reported previously [22]. Phase identification was conducted by fitting the whole powder diffraction pattern according to the Rietveld refinement method using TOPAS V5 software. During the refinements, the crystallite sizes of the Iridium oxide species have been fixed to the values determined by CO-chemisorption.

TEM, HRTEM, SAED and EDX was performed using a FEI Field Emission gun Tecnai G2 F20 S-TWIN microscope operated at 200 kV. Morphological and structural characterization was gained from TEM and HRTEM images. The lattice parameters were calculated *via* Fourier transform analysis of the HRTEM images. Histograms and mean particle size diameters were calculated from measurement of 100 to 400 particles from TEM and HRTEM images. Energy dispersive X-ray spectroscopy (EDX) in nanoprobe mode was used to analyze the composition of the nanoparticles. As in previous studies, the samples were prepared by sonication in ethanol and deposition of the solution onto a holey-carbon film supported on a copper grid, followed by drying.

Catalysts were characterized by Raman spectroscopy. The analyses were undertaken using a Horiba-MTB Xplora spectrometer. The excitation source employed was an Ar ion laser (514.5 nm) operated at 20 mW. The laser was focused on the samples placed on a microscope slide in order to create a spot size with a diameter of ca. 3 µm.

XPS data were collected using a Thermo Scientific K-Alpha$^+$ spectrometer, utilizing a microfocused monochromatic Al$_{K\alpha}$ radiation source operating at 72 W (6 mA x 12 kV). Spectra were acquired using the '400 µm spot' mode of the XPS system at pass energies of 40 eV for high resolution data and 150 eV for survey data, the step sizes were 0.1 and 1 eV, respectively. Charge neutralization was performed using a combination of low energy electrons and low energy argon ions which resulted in a C(1s) energy of 284.8 eV, this gave rise to the Si(2p) at 103.5 eV, Al(2p) at 74.6 eV and Ti(2p) at 458.8 eV, consistent with those of the bare supports, we consider the experimental uncertainty in these energies to be ±0.2 eV. All data were analyzed using CasaXPS (V2.3.23) after subtraction of a Shirley background, and using Scofield sensitivity factors with a kinetic energy dependence of -0.6. Where applicable, data were fitted using models derived

from bulk compounds, this was particularly the case for the iridium line shapes which exhibit asymmetry and may overlap other elemental regions.

Catalytic performance tests

The catalytic performance for total oxidation of alkanes was studied using a total flow set to 50 ml min^{-1} and 0.1 g of catalyst. The catalyst was pressed and sieved in order to obtain a grain size of 0.3 - 0.75 mm. The catalyst was loaded into a quartz tube micro reactor with an inner diameter of 7 mm. When only one hydrocarbon was used, the feed gas consisted of 0.8% mol. alkane (propane, ethane or methane), 19.8% mol. oxygen and 79.4% mol. helium. If a mixture of alkanes was used (methane/ethane, methane/propane or ethane/propane) the feed gas consisted of 1.6% mol. of the mixture of alkanes (with a 50/50 mol. ratio), 19.7% mol. oxygen and 78.7% mol. helium. The reactor was surrounded by a temperature-controlled oven and the temperature inside the fixed catalyst bed was measured using a thermocouple. The reaction temperature used in the experiments was raised from 150ºC to 450°C until the temperature at which 100% conversion was obtained or the calcination temperature was reached. The analyses were carried out in steps of 25 °C. Prior to the measurements, the catalysts were held for 30 minutes at every step until steady-state was attained. Two consistent analyses were made at each temperature and the results averaged. The outlet gas was analyzed by online injection into a Hewlet-Packard gas chromatograph equipped with a Carbosieve-S and a Porapak Q column. Once the reaction was completed, the oven was switched off and the catalyst was allowed to slowly cool down under a stream of flowing helium.

For stability studies, the catalysts were evaluated at temperatures of moderate conversions and the evolution of the alkane conversion with the time on line was monitored.

Results

Catalytic results

Supported iridium catalysts were tested for the total oxidation of propane (C_3) as a model VOC. Some selected catalysts were also tested for the oxidation of ethane (C_2) , methane (C_1) and mixtures of C_1, C_2 and C_3 alkanes. In all cases the only reaction product detected was CO_2, whereas CO, olefins or other oxygenated compounds were not identified. SiO_2, γ-Al_2O_3 and TiO_2, as well as three commercial ZSM-5 zeolites, were employed as supports, and 2 wt.% Ir was deposited on them in all cases.

Firstly, the supports alone were tested for any activity. Silica was inactive over the temperature range studied (from room temperature to 450ºC). γ-Alumina and the different zeolites could activate propane, but only to a low extent, and conversion did not reach 2%. However, titania could activate propane, achieving a conversion of *ca.* 5% at 450ºC. Therefore, the catalytic activity of Ir/SiO_2, Ir/Al_2O_3 and Ir/zeolites can be assigned solely to the properties of the iridium sites. In the case of the Ir/TiO_2 catalysts the activity of the titania sites also has to be taken into account at temperatures over 450 ºC.

The incorporation of iridium onto the supports led to enhanced catalytic activity for all supports. Catalysts supported on alumina were less reactive than iridium catalysts based on silica, zeolites and titania (Figure 1). In Figure 1 A, the propane conversion of the titania catalysts and the pure titania support is presented. At high temperatures (> 400°C) a contribution of the pure titania support on the activity for propane conversion

is visible. The Ir/Ti550 and Ir/Ti750 catalysts operate in this temperature region. For these catalysts the contribution of the titania supported iridium on the propane conversion can be interpreted as the difference between the propane conversion of the catalysts (Ir/Ti550 and Ir/Ti750) and the propane conversion of the pure titania support (black triangles). We note that, the data presented in Table 1, Figure S1 and Table S1 of the supporting information is based on measurements at lower temperatures (275°C), where the influence of the support alone on the propane conversion is negligible.

The characteristics of the catalysts, as well as data for catalytic performance for propane oxidation, are shown in Table 1.

The most active iridium catalysts were those supported on silica and titania calcined at the lowest temperature (350 °C). Unfortunately, these catalysts initially deactivated, and then achieved stable but reduced performance after several hours (see Supporting Information, Fig. S1 and Table S1). This decreased stability has been reported to be related to exhaustion of some highly reducible iridium species [9]. Conversely, the catalysts calcined at 450 °C, and above, were completely stable, with steady-state conversion maintained for at least 8 h (longer tests were not carried out).

The calcination temperature was shown to have an important influence on the catalytic performance. Regardless of the support, the higher the calcination temperature the lower the catalytic activity.
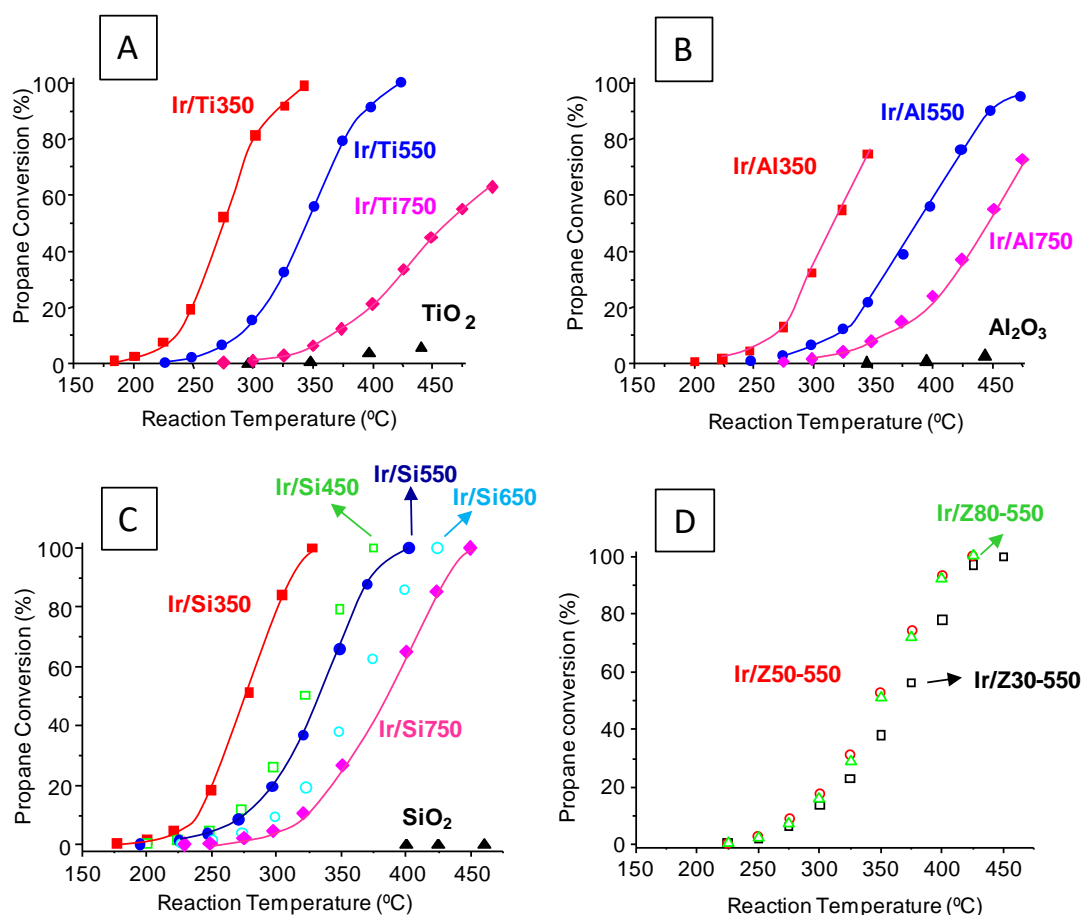
Figure 1. Propane conversion as a function of the reaction temperature for IrOx supported on titania (A), alumina (B), silica (C) and ZSM-5 (D) calcined at different temperatures. Reaction conditions: 0.1 g of catalyst, 50 ml/min, $C_3/O_2/He$: 0.8/19.84/79.36 molar ratio.

For better comparison, Table 1 lists the catalytic performance for the total oxidation of propane of the different catalysts in terms of the catalytic activity obtained at a relatively low single reaction temperature, in order to minimize undesirable mass transfer limitations. Thus, data provided in Table 1 were obtained at 275 ºC, a temperature at which all the iridium catalysts can oxidize propane, but all the supports were inactive. Accordingly, we ensure that the reactivity was due to the catalytic properties induced by the presence of the iridium sites. The results shown in Table 1 refer to the data of the stabilized catalysts.

Table 1. Catalytic properties of the iridium-based catalysts for propane total oxidation.

Catalyst	Calcination Temperature (ºC)	Support	Catalytic activity in C_3 oxidation per Ir atom[a]	TOF[b]
Ir/Si350	350	SiO_2	27.3	127.5
Ir/Si450	450	SiO_2	13.1	93.2
Ir/Si550	550	SiO_2	8.4	104.2
Ir/Si650	650	SiO_2	4.0	62.5
Ir/Si750	750	SiO_2	2.7	63.9
Ir/Ti350	350	TiO_2	33.8	40.3
Ir/Ti550	550	TiO_2	6.6	19.9
Ir/Ti750	750	TiO_2	0.56	11.9
Ir/Al350	350	$\gamma\text{-}Al_2O_3$	5.5	5.5
Ir/Al550	550	$\gamma\text{-}Al_2O_3$	2.6	5.6
Ir/Al750	750	$\gamma\text{-}Al_2O_3$	0.57	1.7
Ir/Z30-550	550	ZSM5, $SiO_2/Al_2O_3=30$	6.7	59.1
Ir/Z50-550	550	ZSM5, $SiO_2/Al_2O_3=50$	10.2	54.4
Ir/Z80-550	550	ZSM5, $SiO_2/Al_2O_3=80$	7.7	76.0

[a] per Ir present in the catalyst at 275 ºC expressed as propane molecules reacted per atoms of Ir in the catalyst per hour.

[b] TOF: turnover frequency. Activity per Ir exposed in the catalyst (determined by CO-chemisorption) at 275 ºC expressed as propane molecules reacted per atoms of exposed Ir in the catalyst per hour.

Apparent activation energies in propane oxidation were estimated using iridium supported catalysts, ranging from 90 to 130 kJ/mol. Catalysts with silica and that with titania calcined at 350ºC present an activation energy between 90-100 KJ/mol. Catalysts

with alumina show activation energies between 105 and 130 kJ/mol. Those with alumina and titania calcined at 750ºC present values of ca. 130 kJ/mol. So, a rough inverse relationship between activation energy and catalytic activity has been observed.

Different experiments were undertaken with methane, ethane and mixtures over the Ir/Ti550 catalyst (Table 2), in order to assess the reactivity for other short chain alkanes. In all cases, performance was stable with the time on-line and alkane conversions did not vary up to at least 8 h reaction. On the other hand, as expected, the higher the alkane chain length, the greater the activity of the catalyst. For the total oxidation of alkanes the activation of the C-H bond is the rate determining step. Therefore, the reactivity is inversely related to the energy of its weakest C-H bond, resulting in methane as the most stable alkane followed by ethane and propane [3]. In independent experiments, the reaction rate observed for ethane oxidation was approximately twice that of methane. However, the reaction rate for propane oxidation was 4-5 times higher than that of ethane.

In most cases, the reaction rates for mixtures of alkanes decreased, although this decrease was often not very large. In the methane + ethane mixture a slight decrease was observed for the activity (10-20%), compared to independent experiments feeding only one alkane. For an ethane + propane mixture, a decrease of 20-30% in the reaction rate took place in both cases. This lowering of activity could be due to competitive adsorption on the catalyst. In the methane + propane mixture different behavior was observed, as propane reactivity was barely modified compared with experiments with propane alone, whilst methane decreased by 30% conversion compared to when it was fed alone. This decreased methane activity in the mixture with propane can be related to the competitive adsorption of both alkanes and to the fact that propane adsorbs more strongly at lower reaction temperatures. Propane is likely to be less affected by the

presence of methane, because of the low adsorption of methane at the temperatures propane was activated [37], [38]. Therefore, the simultaneous presence of different hydrocarbons exerts a subtle suppression of activity. This decrease was less pronounced for the most reactive hydrocarbon of the mixture, if the difference in reactivity of the alkanes was high.

Table 2. Influence of the nature of the alkane on the catalytic activity per active site on the Ir/Ti550 catalyst at 325 ºC[a].

	Reaction rates (molecules C_x $atom_{Ir}^{-1}$ h^{-1})			Relative rates
	Methane	Ethane	Propane	$r_{C1}/r_{C2}/r_{C3}$
Independent experiments	5.1	9.0	38.7	1/1.8/7.6
Mixture C_1+C_2	4.3	8.1	-	1/1.9/-
Mixture C_2+C_3	-	6.2	32.7	-/1/5.3
Mixture C_1+C_3	3.8	-	38.5	1/-/10.1

[a] Reaction conditions in text. Data expressed as alkane molecules reacted per atom of Ir in the catalyst and per hour.

Three consecutive cycles of testing with the same catalyst were carried out with the Ir/Ti550 catalyst using standard conditions and reproducible stable performance was observed (Figure 2A). Additional experiments were undertaken adding water vapour and/or CO_2 to the mixture in order to check the influence of the presence of these compounds in the mixture, as they are often present under industrial conditions (Figure 2B). Water concentrations up to 2.5 mol. % did not affect the propane conversion, whereas a slight decrease was observed when 5 mol. % was added. The presence of low amounts of CO_2 in the feed did not lead to appreciable changes in the catalytic

performance. Cessation of the water feed resulted in restoration of the catalytic performance to the initial level. Therefore, this catalyst is highly robust, showing stable catalytic behaviour in the presence of CO_2 and/or with moderate amounts of water in the feed.
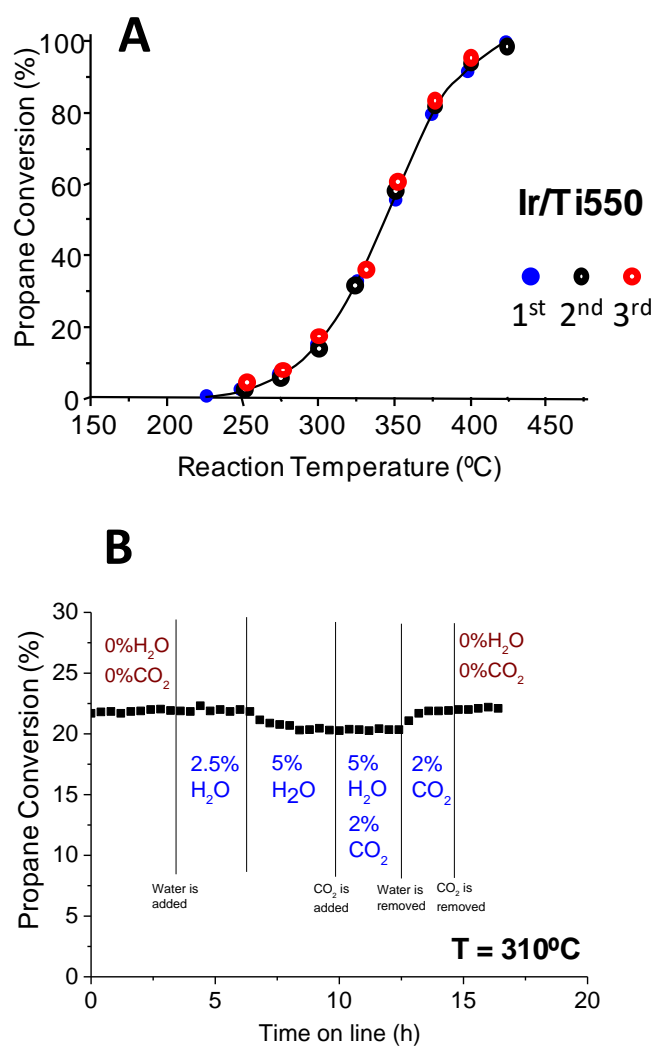
Figure 2. (A) Evolution of propane conversion with reaction temperature for Ir/Ti550 in 3 consecutive cycles. (B) Influence of the presence of water and/or CO_2 on the propane conversion. Reaction conditions: 0.1 g of catalyst, 50 ml/min, $C_3/O_2/He$: 0.8/19.84/79.36 molar ratio.

Table 3. Physicochemical properties of the iridium catalysts.

Catalyst	Surface area ($m^2 g^{-1}$)	Dispersion[a] (%)	Particle Size[a] (nm)	B.E. Ir $4f_{7/2}$ XPS (eV)
Ir/Si350	174	21.4	5.2	61.6 (61.1)[b]
Ir/Si450	173	14.1	7.8	61.6
Ir/Si550	177	8.1	13.7	61.8
Ir/Si650	171	6.4	17.2	61.9
Ir/Si750	168	4.2	26.7	61.8
Ir/Ti350	52	84.0	1.3	61.1 (61.3)[b]
Ir/Ti550	51	33.1	3.4	61.1
Ir/Ti750	15	4.8	23.2	61.1
Ir/Al350	177	98.3	1.0	61.6 (61.8)[b]
Ir/Al550	172	47.0	2.3	61.4
Ir/Al750	166	32.8	3.4	61.5
Ir/Z30-550	397	11.4	9.7	61.6
Ir/Z50-550	406	18.7	5.9	60.9
Ir/Z80-550	410	10.1	10.9	n.d[c]

[a] mean size in nm and iridium dispersion by CO chemisorption considering CO/Ir at. ratio of 2 and spherical shape; [b] in brackets values for used catalysts; [c] not determined.

Characterization results

The catalysts have been characterized by a series of techniques to establish their bulk and surface characteristics to elucidate possible causes for the different catalytic performance. The addition of iridium to the supports (silica, titania, γ-alumina and ZSM-5) led to a slight decrease in the surface area with respect to the pure supports (Table 3). Silica had a surface area of 181 $m^2 g^{-1}$, which slightly decreased when iridium was added. Addition of iridium to the alumina support, resulted in a small decrease of surface area from 178 $m^2 g^{-1}$ to 165 $m^2 g^{-1}$. A similar observation was made for the titania catalysts, where the surface area dropped from 55 $m^2 g^{-1}$ to 50 $m^2 g^{-1}$ for the

iridium catalysts calcined at 350 and 550 ℃. However, the calcination at 750 ℃ resulted in a significant reduction of the surface area (15 $m^2 g^{-1}$). The silica support was calcined at 800°C before the addition of iridium and subsequent calcination. Therefore, the decrease in surface area of the silica supported catalysts does not most likely originate from Ostwald ripening. For these supports, the slight decrease in surface area with addition of iridium might originate from filling of pores of the support by the iridium oxides. For titania supported catalysts calcined at high temperature, the filling of the pores cannot account for the change in surface area. In this case, a change of surface area of the support is most likely the reason for the relevant decrease in BET surface area after addition of iridium and subsequent calcination.

The structure of the supports and the IrOx phase was investigated with powder X-ray diffraction (Figure 3). For the alumina, silica and zeolite supported catalysts, all diffraction peaks associated with the support remain unchanged for all calcination temperatures. In the titania catalysts it was observed that heat-treatments at 350 and 550 ℃ did not modify the phases of the titania support, which was originally present mainly as anatase (JCPDS: 21-1272) with a lower amount of rutile (JCPDS: 21-1276). However, the calcination at 750 ℃ resulted in almost complete transformation of the anatase phase into rutile. This was in agreement with the drastic decrease in the surface area observed when the Ir/titania catalyst was heat-treated at 750 ℃. We note that neither γ-Al_2O_3 nor anatase TiO_2 are thermodynamically stable phases at high temperatures. Thus, the transition to α-Al_2O_3 takes place at high temperatures [39] and although the kinetics of this phase transition are slow [39], this structural transformation requires only small energy differences [40] and begins at approximately 750 °C. In our case no change of the alumina phase was observed when calcined at 750 ℃. In the case of the titania support, initially consisting of rutile and anatase, rutile is the

thermodynamically stable phase, and anatase transforms to rutile irreversibly and slowly at temperatures over 600 °C [41]. In fact, for the titania catalyst calcined at 750 ºC anatase was almost completely transformed into rutile (rutile 95 wt.% and anatase 5 wt.% according to Rietveld refinements).

The structures and simulated diffraction patterns of iridium metal, corundum like Ir_2O_3 and rutile IrO_2, possible IrOx species, are presented in Figure S2 of the Supporting Information. Unfortunately, the most intense diffraction peak of Ir_2O_3 (2-10) overlaps with the (101) peak of IrO_2, which complicates phase identification. Therefore, a whole pattern fitting according to the Rietveld method has been applied for phase identification of the IrOx species present in the catalysts. The calculated diffraction patterns are included in Figure 3 as thin black lines for each catalyst. Since nano-particles show very broad X-ray reflections, which may become undiscernible from the background, only the catalysts with particle sizes > 4 nm as determined by CO-chemisorption are discussed (compared to Table 3). The Rietveld refinements for all catalysts show IrO_2 (JCPDS 00-043-1019) as the main IrOx species. The presence of a corundum like Ir_2O_3 structure or iridium metal for silica supported catalysts calcined at low temperature (350°C and 450°C) cannot be completely ruled out.
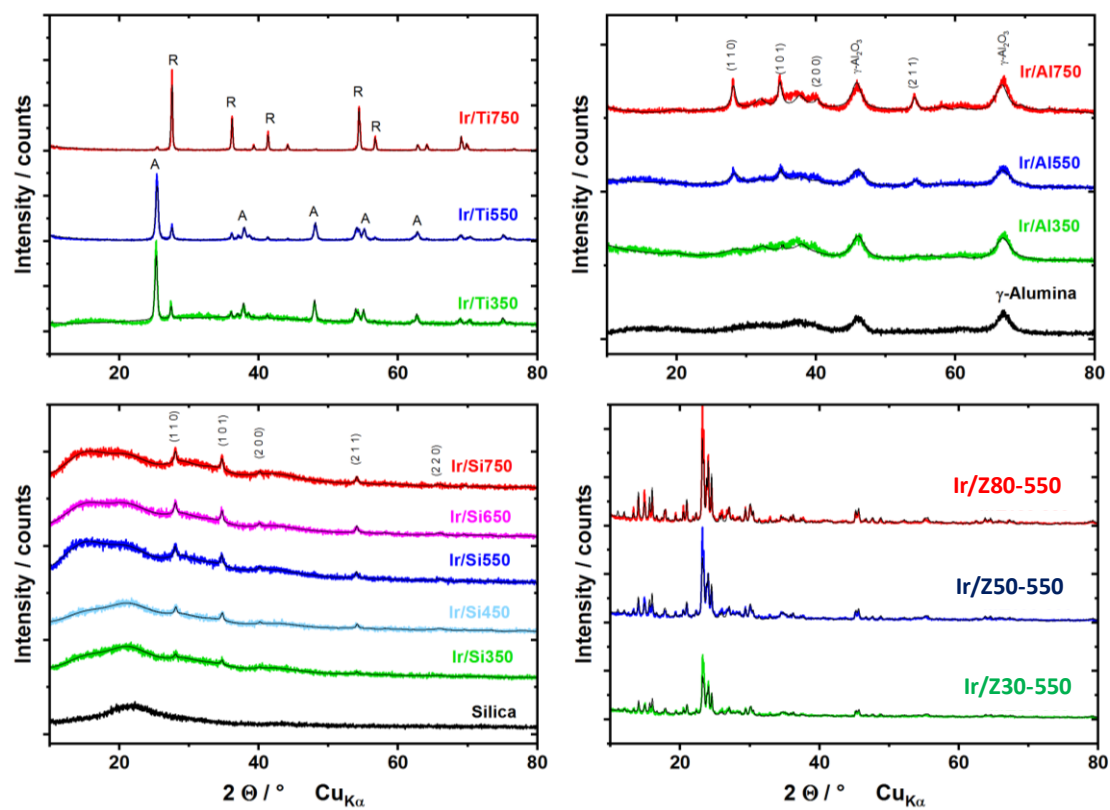
Figure 3. XRD patterns of Ir catalysts supported on titania, γ-alumina, silica and ZSM-5. Symbols: A corresponds to anatase TiO_2, R: rutile TiO_2, γ: γ-Al_2O_3.

TEM images of titania, alumina and silica supported catalysts are presented in Figure 4.
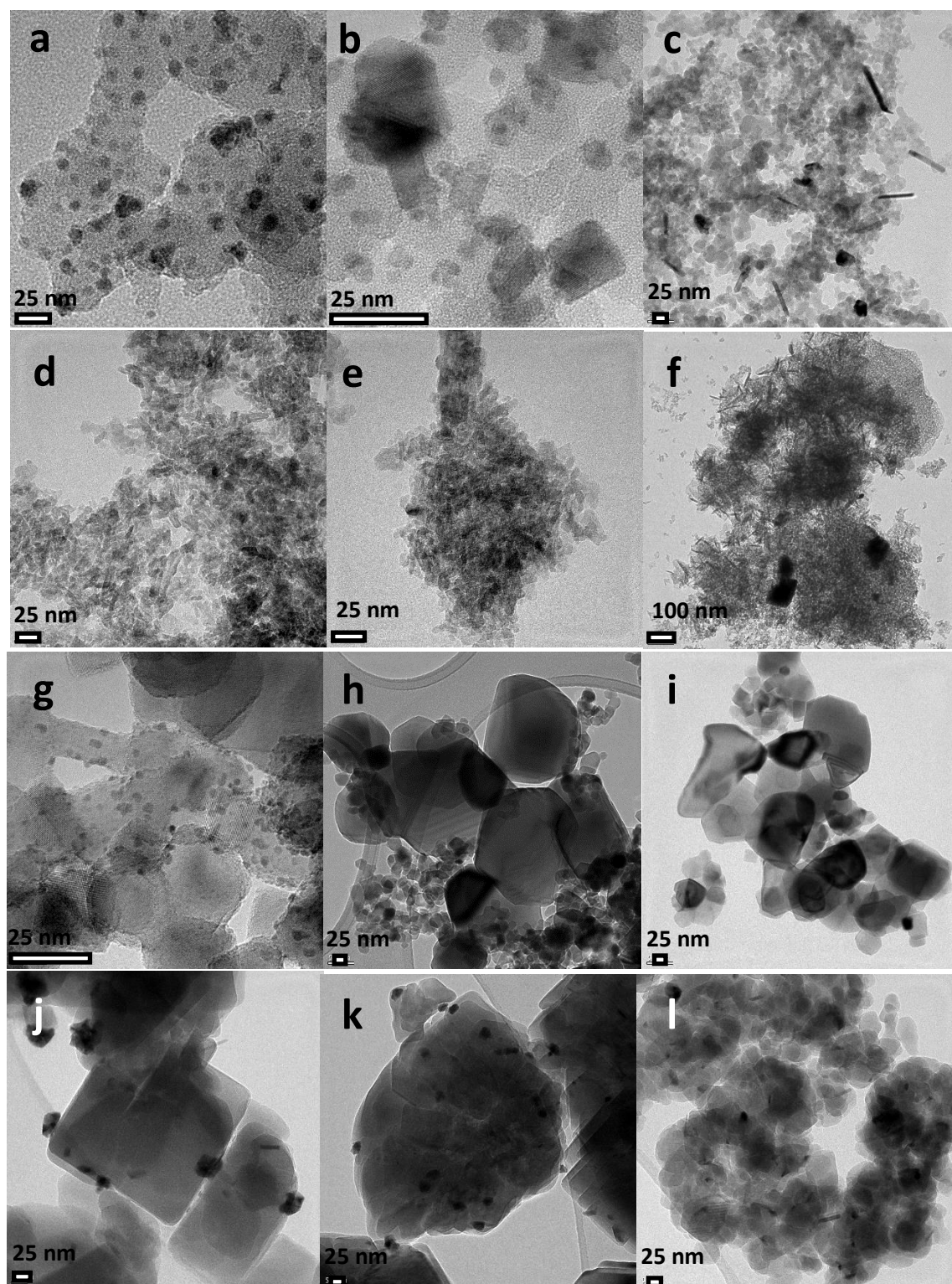
Figure 4. TEM images for Ir/Si350 (a), Ir/Si550 (b), Ir/Si750 (c), Ir/Al350 (d), Ir/Al550 (e), Ir/Al750 (f), Ir/Ti350 (g), Ir/Ti550 (h), Ir/Ti750 (i), Ir/Z30-550 (j), Ir/Z50-550 (k), Ir/Z80-550 (l) catalysts.

For all catalysts investigated with TEM, the presence of iridium has been confirmed with energy dispersive X-ray spectroscopy (see Figure S3). A detailed analysis of large areas of the samples confirm that the overall iridium loading for all the catalysts was in the 1.9 to 2.2 wt.% range. The effect of the calcination temperature and also the nature of the support are important to control the dispersion of nanoparticles. For all supports, an increase in the IrOx-particle size has been observed when the calcination temperature increased. Histograms from measurements of the particle size of 100 to 400 iridium particles for titania, alumina and silica supported catalysts calcined at 350°C are shown in Figure S4 of the Supporting Information. Regarding the nature of the support, the smallest particles correspond to the catalyst supported on alumina and the largest to the catalyst supported on silica. Due to the low contrast between the support and the iridium oxide, we were not able to reliably determine a particle size distribution of titania and alumina supported catalysts calcined at higher temperatures.

Interestingly, IrOx particles present different morphologies. Most of them are spherical (or quasi spherical with a pseudo-tetrahedral shape), whereas in some catalysts calcined at high temperatures (Ir/Si750 and Ir/Al750) elongated rod particles are clearly observed. Table S2 shows a summary of the different morphologies observed. Ir/Si750 catalyst (Fig. 4c) shows spherical particles with a mean diameter of *ca.* 20 nm. The analysis of rod like structures resulted in an average length of about 60 nm and an average diameter (thickness) of 12 nm. As in the case of the Ir/Si750, in the Ir/Al750 (Figure 4f) spherical and elongated particles are present, although they are more randomly distributed. Overall, iridium is evenly distributed throughout the whole sample. At calcination temperatures below 550°C, iridium is well dispersed. In the catalysts calcined at 750°C, a few large spherical particles of *ca.* 10-15 nm and a few

elongated ones (80 nm length and 15 nm thickness) were also observed. In Ir/Ti750 only spherical particles, mainly in the 30-40 nm range, were observed.

To further elucidate the nature of the iridium phases present in the different catalysts, HR-TEM analysis has been undertaken (Figure 5 and S5). For several IrOx particles of each catalysts the spacing of atomic planes has been analyzed with profile plots and fast Fourier transformation (FFT) techniques. Lattice parameters of cubic and tetragonal phases were calculated by using the following formula:

$$\frac{1}{d^2} = \frac{h^2 + k^2 + l^2}{a^2} \text{ (cubic phase)}$$

$$\frac{1}{d^2} = \frac{h^2 + k^2}{a^2} + \frac{l^2}{c^2} \text{ (tetragonal phase)}$$

where h, k and l are Miller indices. a and c are lattice parameters. Table S2 summarizes the lattice parameter of cubic Ir and tetragonal IrO_2 phases measured from $d_{(hkl)}$ interplanar distances, using formula 1 and 2, of the different samples in comparison with data cited in JCPDS database: file 046- 1044 and 01-086-0330 corresponding to cubic Ir and tetragonal IrO_2, respectively.

Analysis of HRTEM images and the corresponding FFTs showed the crystalline structure of IrO_2 in all samples. Catalysts calcined at 550°C and above show exclusively crystal fringes of 1.59 Å, 2.58 Å and 3.21 Å, which can be assigned to the lattice spacing of (220), (101) and (110) family planes of tetragonal IrO_2 (JCPDS 01-086-0330). These nanoparticles are maintained with subtle shifts in the a and c lattice parameters of the tetragonal IrO_2 structure when coalescence occurs. Additionally, for the catalysts treated at 350°C (Ir/Si350, Ir/Al350 and Ir/Ti350), apart from IrO_2 particles, some crystal fringes of 2.21 Å are also detected. These can be assigned to the

(111) family planes of iridium metal, although the presence of (2-13) family planes of corundum like Ir_2O_3 cannot be completely ruled out. Anyway, we can note with certainty that a reduced IrOx is present on our alumina, silica and titania supported catalysts when calcined at 350°C. We must mention that these reduced IrOx species (metallic Ir) are located in close contact with IrO_2 particles. In our previous report, we were able to connect the initial deactivation during reaction conditions of the Ir/Si350 catalyst with the exhaustion of reduced Ir species [9]. Interestingly for all catalysts calcined at 350°C (silica, alumina and titania) the exhaustion/oxidation of the iridium reduced species is observed after use in catalysis, which can be related to the deactivation observed in the oxidation of alkanes. It must be noted that no spacing corresponding to the iridium salt employed in the preparation method of these catalysts (Ir acetyl acetonate) has been detected in any of the studied catalysts.
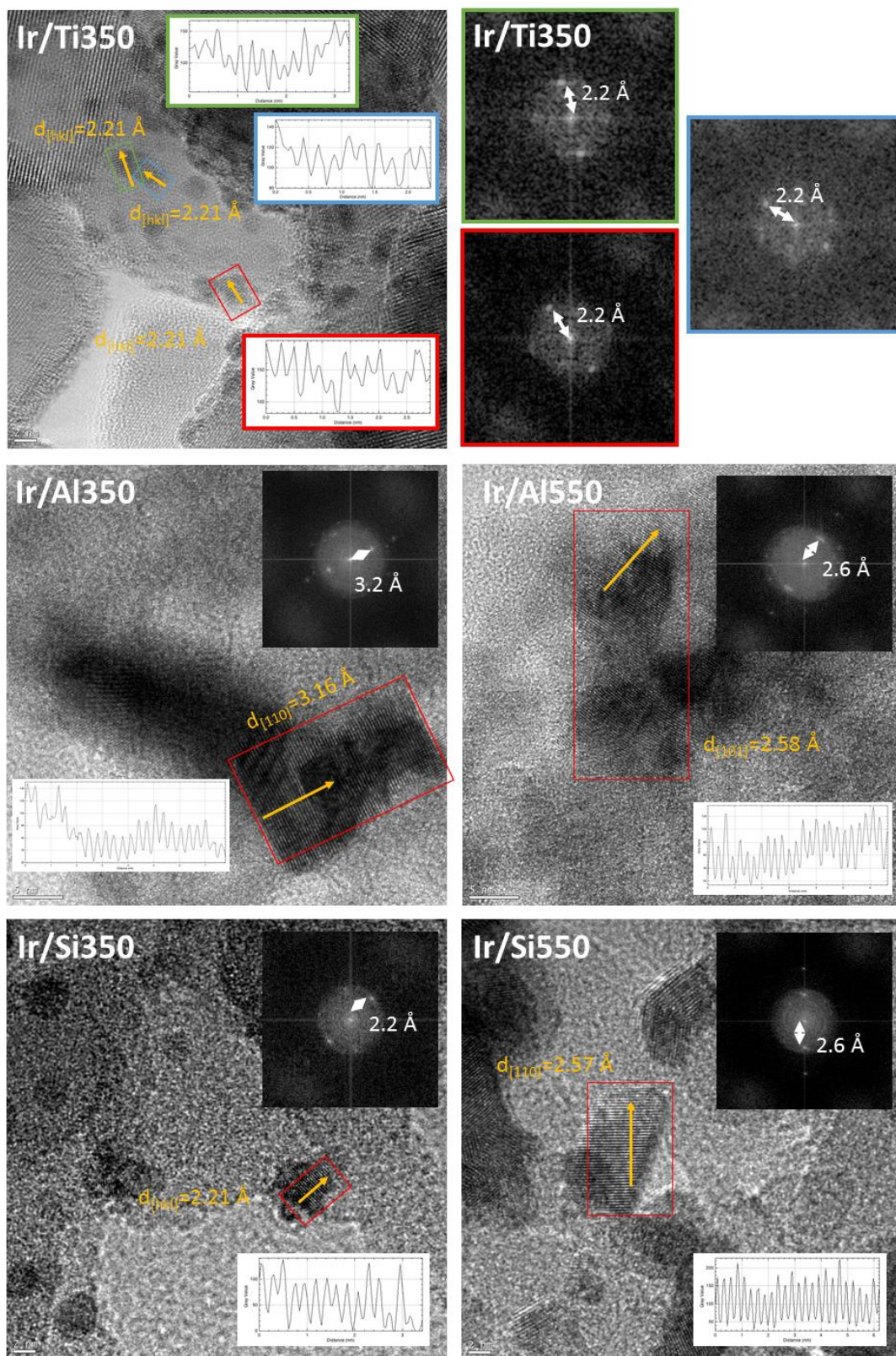
Figure 5. HR-TEM images of selected Ir-catalysts. Spacing of the atomic planes has been analyzed with profile plots and FFT, both presented as insets in the respective HR-TEM image. The direction and the calculated spacing of the atomic planes are included as well.

EDX-mapping shows in all cases a good distribution of iridium (as metallic Ir and/or IrO$_2$ nanoparticles) on the supports, especially in the catalysts heat-treated at 350 and 550ºC. The samples calcined at 750ºC also present IrO$_2$ nanoparticles highly dispersed on the supports, but with some agglomeration and coalescence of the nanoparticles. Figure 6 shows the EDX-mapping of some representative catalysts.
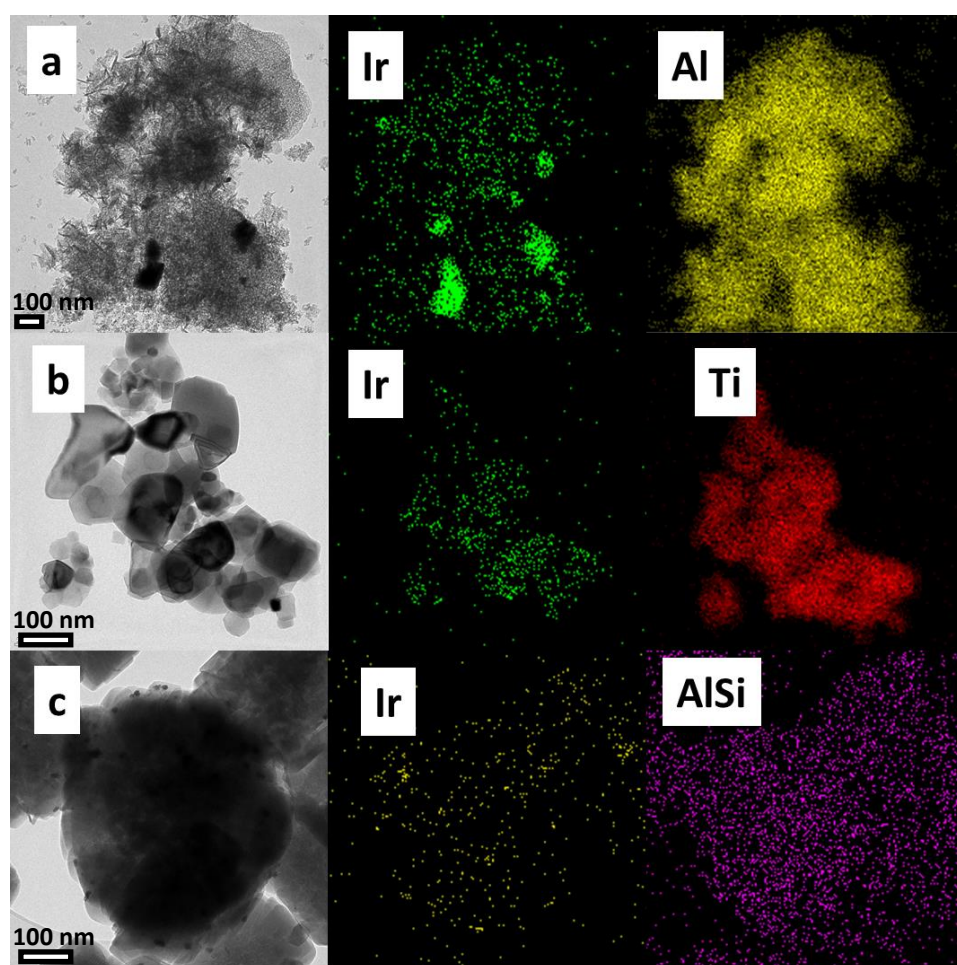
Figure 6. TEM-EDX mapping of IrOx supported catalysts; Ir/Al750 (a), Ir/Ti750 (b) and Ir/Z100-550 (c).

CO chemisorption experiments were undertaken in order to measure the Ir dispersion and the number of active surface iridium sites [42]. It was assumed that the particles had spherical shapes and the CO-Ir interaction took place with a CO:Ir stoichiometric factor

of 2 [43,44]. The results obtained (see Table 3) corroborated the information suggested by microscopy, as iridium dispersion on silica catalysts was the lowest, and alumina the highest, the order was:

$$silica < ZSM\text{-}5 < titania < alumina$$

It was also observed that the increase of the calcination temperature decreased the iridium dispersion. This decrease in the iridium dispersion with the heat-treatment temperature was marked for the titania catalyst at 750ºC. This sharp decrease was related to the drop of the surface area of the support, as anatase transforms into low surface area rutile, favoring agglomeration as discussed earlier. For the alumina catalyst calcined at 350 ºC a dispersion close to 100% was obtained. It is worth commenting that this high theoretical value was estimated assuming the usual CO-Ir factor of 2 and this factor could be different for very small particles. McVicker *et al.* [45] demonstrated that the CO:Ir ratio depends on the level of aggregation of the iridium species; iridium species with low aggregation adsorb more CO molecules per Ir atom than large clusters of iridium. What is more, in the case of H_2 chemisorption it has been reported that the H_2:Ir stoichiometry varies with the size of the iridium particles from 2.6 in small particles (dispersions over 90%) to 2.0 in larger particles [46].

The reducibility is an important factor to exert control in reactions that take place through a redox mechanism. In fact, it has been proposed that propane oxidation on Ir/silica catalysts takes place through a redox mechanism [9]. Accordingly, Temperature Programmed Reduction (TPR) experiments were undertaken on these catalysts (profiles are shown in Figure 7). The interpretation of the reduction profiles were not straightforward as there were several overlapping features, which in some cases were not well defined. In the silica series [9] there were 3 types of features at *ca.* 120, *ca.* 195

and *ca.* 330 ºC, corresponding to IrOx species interacting weakly, medium and strongly with the support. The intensity of the low temperature feature was highest in the sample calcined at 350 ºC and decreased as the calcination temperature increased. In the case of the titania series (Figure 7A) the profile of the sample calcined at 350 ºC presented a main reduction feature at very low temperature (74 ºC), and a second one at *ca.* 200 ºC. In the titania supported catalyst calcined at 550 ºC (Ir/Ti550) the main feature presented a maximum at 139 ºC, whereas the titania supported sample calcined at 750 ºC (Ir/Ti750) presented the maximum at 260 ºC. Therefore, a clear shift to higher reduction temperatures was observed when increasing the calcination temperature. It must be noted that the titania sample calcined at 350 ºC after use presented a pattern different to that of the fresh sample. Thus, the low temperature reduction at 74 ºC shifted to 112 ºC (see Figure 7A). This modification of the reduction behavior can be related to the presence in the fresh catalyst of reduced IrOx species in close contact with IrO_2, and was in agreement with microscopy results. The close proximity of these reduced IrOx species with IrO_2 facilitates the reduction of the IrO_2 surface species *via* spill-over of adsorbed atomic hydrogen. Conversely, the titania sample calcined at 550 ºC after use did not present appreciable differences compared to the fresh one. This different behavior can be related to the different catalytic stability observed. As shown in Figure 2A and Figure S1 of the Supporting Information, the titania supported sample calcined at 550 ºC (Ir/Ti550) was fully stable for at least 3 catalytic cycles, whereas the one calcined at 350 ºC (Ir/Ti350) promptly deactivated with time on line, although after 4 h on line the propane conversion did not decrease any further.

The alumina catalysts showed lower reducibility than those of silica or titania (Figure 7B). For the catalysts calcined at 350 °C and 550 °C the main reduction feature was centered at *ca.* 220 ºC. Moreover, a wide feature at lower temperatures, with a

maximum at 120 ºC, was detected in the sample heat-treated at 350 ºC. The sample heat-treated at 750 ºC had a similar shape to that heat-treated at 550 ºC but displaced to higher temperatures. Similarly, the three catalysts based on the ZSM-5 support presented one main reduction feature at 200-215 ºC (Figure 7C).
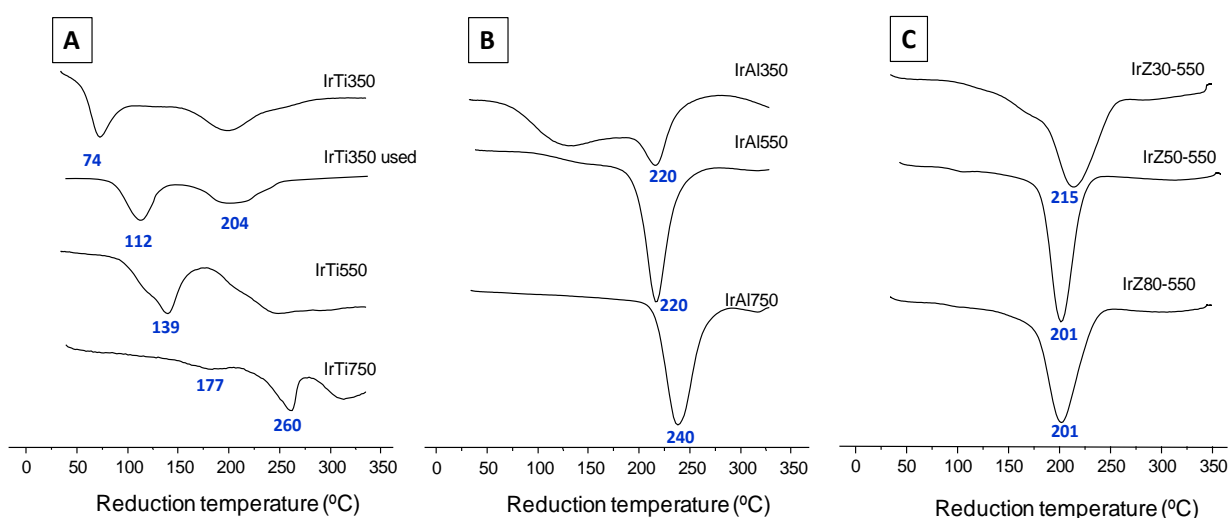

Figure 7. TPR profiles of Ir catalysts supported on (A) titania, (B) alumina, and (c) ZSM-5 zeolites.

XPS analysis of all samples (Figure 8) revealed the characteristic asymmetric line shapes of IrO_2 for Ir(4f) peaks in all samples. Note the Ir(4f) region overlaps with the Ti(3s) region of TiO_2, so fitting was achieved using model spectra acquired from an untreated P25 TiO_2 sample, and the concentration of iridium derived from the 4f peaks compared with that derived from the equivalent (4d) peaks. This gave a confidence limit of ± 0.2 at.% in the Ir derived atomic concentrations.

The binding energy for bulk IrO_2 is 61.9 eV [47] with the present catalysts showing a range of values down to *ca.* 1 eV below this bulk value. Evident from the binding energies was that acidic SiO_2 and Al_2O_3 supports retained a high, bulk-like binding

energy for the IrO$_2$, whilst TiO$_2$ and ZSM-5 tended to have a lower binding energy. In the case of TiO$_2$ catalysts the binding energy was very close to the value observed for metallic Ir, although there was no evidence for the formation of metallic Ir from the photoelectron spectra. With respect to this point, we note our earlier comment, which indicated small quantities of metallic Ir observed *via* TEM, the lack of metallic content in the XPS can therefore be ascribed to poor dispersion or a significant oxide shell on a metallic Ir core. The lowering of the binding energy in TiO$_2$ catalysts could be interpreted as the result of an interaction with the support and the formation of electron rich Ir centers. We note that the Ir/Al350 sample had a second type of species (magenta peaks) at higher binding energy, which could be related to different Ir species, maybe interacting with a different site, or maybe due to a lower particle size.
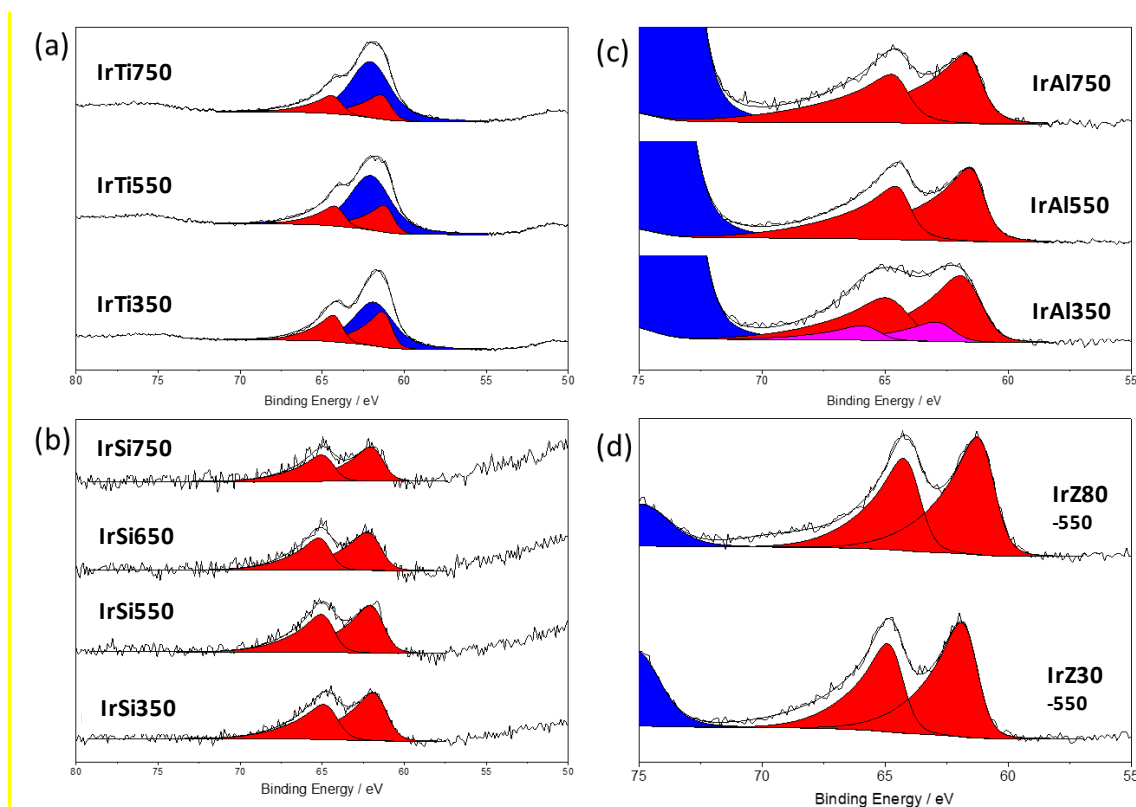

Figure 6. Ir(4f) core level spectra for (a) Ir/Titania, (b) Ir/Silica, (c) Ir/Alumina and (d) Ir/Z series of fresh catalysts. Note: Red indicates Ir(4f) peaks, whereas blue represent overlapping or neighboring peaks such as Ti(3s) and Al(2p). Magenta peaks correspond to unidentified species.

Characteristics of Ir-O bonds were investigated by Raman spectroscopy as presented in Figure S6 of the Supporting Information. The typical Raman spectrum of pure IrO_2 has intense bands corresponding to A_{1g} (750-760 cm^{-1}) and E_g (550-570 cm^{-1}) symmetries, and weak bands of B_{1g} (145 cm^{-1}) and B_{2g} (728 cm^{-1}) symmetry modes [48]. Accordingly, we clearly detected the bands corresponding to E_g and A_{1g} symmetries, but only for the catalysts supported on alumina, silica and ZSM-5 zeolites. Figure 9 shows the Raman spectra of these catalysts in the 500 to 800 cm^{-1} range. The most interesting feature observed was the drastic difference between the positions of the IrO_2 bands depending on the support. The E_g and A_{1g} mode bands of IrO_2 shifted to lower frequency in the silica catalysts compared to those with alumina. This displacement was significant (*ca.* 10 cm^{-1}) and likely implied longer bonds in silica than in alumina catalysts. Consequently, the Ir-O bond strength must be markedly lower in the silica catalysts. Finally, we must indicate that, for both supports, a very slight shift to higher frequencies was observed when the calcination temperature increased. In the case of the catalysts supported on the zeolites an intermediate behavior was observed, although more similar to that of silica catalysts.

In the case of the Ir/TiO_2 catalysts, no iridium oxide peaks were detected, likely due to the high intensity of bands of the support that overlapped with iridium bands, which presented lower intensity due to low loading (2 wt.%). The pure titania support, and those Ir/TiO_2 catalysts heat-treated at 350 and 550 ºC, presented typical spectra of anatase with the most intense absorption bands centered at *ca.* 395, 515 and 635 cm^{-1}. The catalyst calcined at 750 ºC presented the main absorption bands at *ca.* 435 and *ca.* 610 cm^{-1}, which are characteristic of the rutile phase. This is in good accordance with the XRD results.
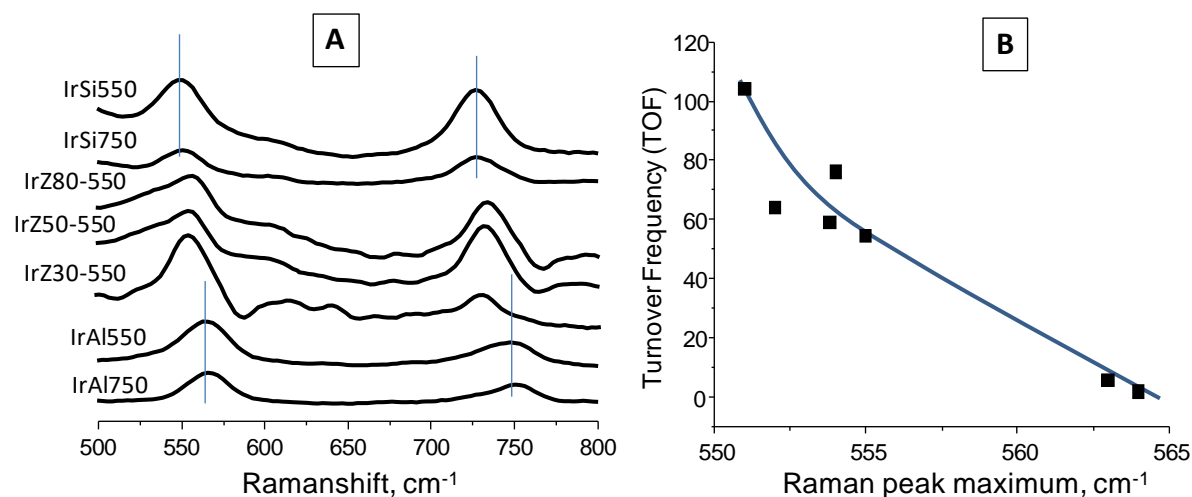
Figure 9. Raman spectra of Ir catalysts supported on silica, alumina and ZSM-5 zeolites (A) and relationship between the TOF in propane oxidation with the position of the maximum of a representative Raman band of IrO_2 (B).

Discussion

Firstly, we want to mention that no direct link can be observed between the catalytic activity and the surface area of the catalysts. In fact, catalysts based on silica are highly active in contrast with those of alumina in spite of the fact that the surface area in both cases is in the same range.

To determine a possible particle size effect and the effect of the support on the activity of the catalysts, the catalytic propane total oxidation activity normalized for total Ir content (considering all the Ir atoms present in the catalyst) is plotted over the particle size as determined by CO chemisorption in Figure 10. Each point in Figure 10 represents one catalyst applied for the total oxidation of propane at a reactor temperature of 275°C. As mentioned earlier, for this reaction temperature, all catalysts are active and operate in the kinetic regime and the absence of any mass transport limitations can be assumed. For all catalysts, a decrease in activity per Ir atom with increasing particle size is apparent (Figure 10), although the catalysts with different

supports follow different trends. Interestingly, silica and zeolite supported catalysts show the highest activity, even though they exhibit the lowest dispersion (see Table 3). In fact, it is observed that the nature of the support is a determining factor, with silica having the highest catalytic activity at a fixed particle size. Titania catalysts calcined at 350 and 550ºC also have comparable overall activity to those of silica, although for a given particle size the activity observed is lower.
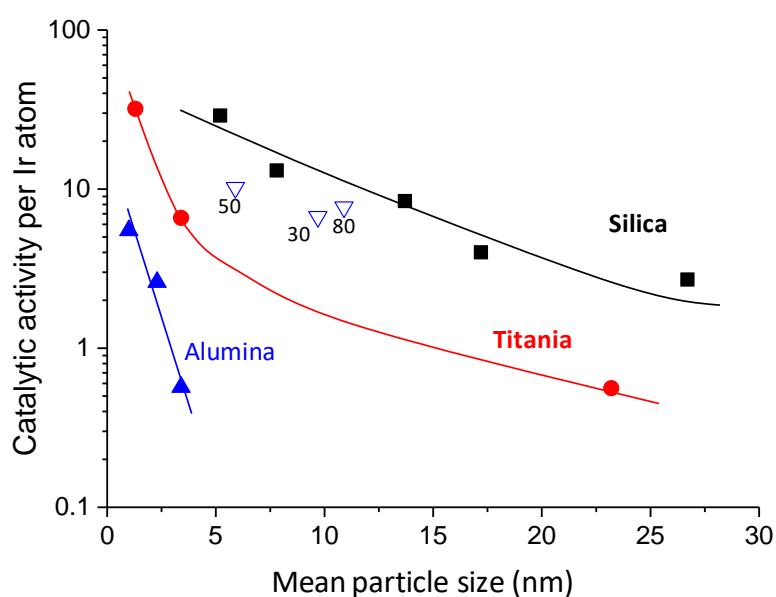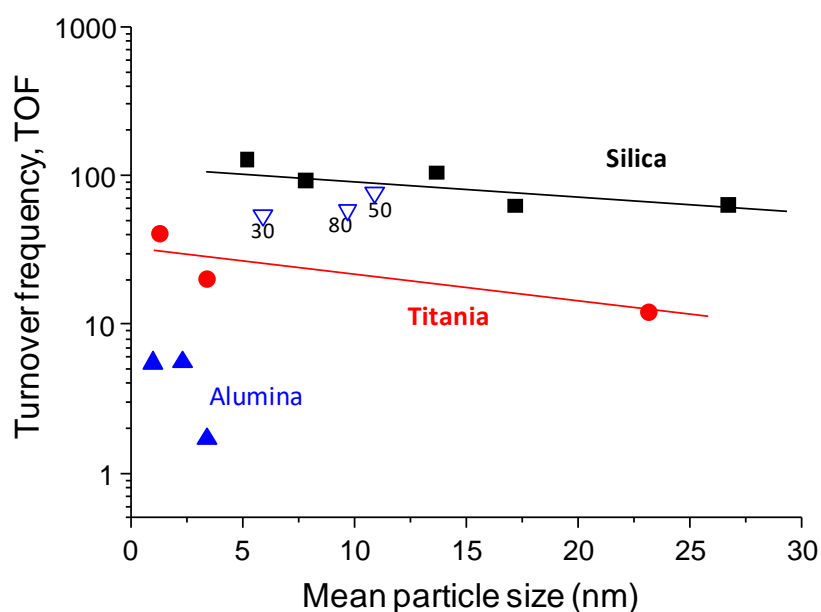

Figure 10. Influence of the mean particle size of iridium on the catalytic activity per Ir-atom in the total oxidation of propane. Symbols: (■) Ir/Silica, (●) Ir/Titania, (▲) Ir/Alumina, (v) Ir/Z catalysts. Notes: Reaction conditions in text and 275 ºC. Catalytic activity per Ir atom as molecules of propane reacted per Ir atom and per hour.

Since only the surface of the heterogeneous catalyst is exposed to the reactant, the catalytic activity was further normalized to the number of Ir surface sites. In Figure 11 the catalytic activity per exposed Ir atom (Turnover frequency, TOF) is plotted over the particle size. Each point in Figure 11 represents one catalyst applied for the total

oxidation of propane at a reactor temperature of 275°C. Overall, the TOF of the supported catalysts is dominated by the influence of the support and follows the trend

alumina < titania < ZSM-5< silica.

Within a series of a certain support, the turnover frequency decreases with increasing particle size. This is contrary to reports on Pd and Pt catalysts, for which the catalytic activity increases with increasing particle size [34], [35].

Figure 11. Influence of the mean particle size of iridium on the catalytic activity normalized for exposed surface Ir-atoms in the total oxidation of propane. Symbols: (■) Ir/Silica, (●) Ir/Titania, (▲) Ir/Alumina, (v) Ir/Z catalysts. Notes: Reaction conditions in text, reaction temperature 275 ℃. Turnover frequency, TOF, as molecules of propane reacted per exposed Ir atom per hour.

The total oxidation of propane on iridium catalysts proceeds by a redox mechanism [9], hence the reducibility of the Ir sites must play a major role. It should be commented on that re-oxidation of iridium is not likely to be the rate determining step, since the

oxidation of Ir^0 to IrO_2 takes place at temperatures close to room temperature [49]. In fact, iridium has the highest metal-O bond energy compared to other noble metals (Pd, Rh, Ir, Pt) [50]. In our catalysts iridium is mainly present as IrO_2, which is active for alkane oxidation, although it presents the drawback compared to metallic Ir, that it cannot adsorb alkanes at low temperatures [51].

To further shed light on the origin of the different catalytic behavior, we turn once more to our physiochemical characterization. XRD and HR-TEM investigations show that IrO_2 is the main iridium species present in all catalysts. Additionally, both techniques individually provide evidence for a more reduced IrOx (likely Iridium metal) species present on alumina, titania and silica supported catalysts calcined at 350°C.

The characteristics of the bulk Ir-O bonds have been investigated with Raman spectroscopy. A significant shift towards lower frequency of the E_g and A_{1g} bands of IrO_2 has been observed for silica supported catalysts compared to those supported by alumina (Figure 9B). Most likely, this shift is caused by an increased Ir-O bond length and hence a decreased Ir-O bond strength in silica supported catalysts (compared to alumina supported ones). Catalysts with weak Ir-O bonds allow easier lattice oxygen removal, and consequently higher activity in reactions that take place through a redox Mars-Van-Krevelen mechanism, as this is the case for the alkane total oxidation on iridium catalysts [9]. This is further supported by the good correlation between the maximum of the E_g Raman shift and the TOF of the tested silica, ZSM-5 and titania supported catalysts (Figure 11 B). For all three supports, with increasing calcination temperature slight shifts towards shorter and stronger Ir-O bonds were observed from Raman spectroscopy.

The near surface region of the IrOx particles has been characterized with XPS. In all cases, iridium is present as Ir^{4+} species, although different shifts are observed depending on the support. Silica and alumina supported catalysts retain a bulk like binding energy for IrO_2, while the Ir(4f) binding energies of titania and ZSM-5 supported catalysts are decreased by *ca.* 1eV. The lowering of the binding energy could be interpreted as the result of a strong interaction with the support and the formation of electron rich Ir centers. Unfortunately, with the XPS results obtained in the present article no direct correlation between the binding energies or the iridium oxidation state with the catalytic activity has been found.

The reducibility of the catalysts has been determined with H_2-TPR. Overall, it is observed that the reduction of the iridium species of these catalysts takes place at least through three different steps associated with Ir species. The temperature programmed reduction profiles obtained are complex and a direct link between the reducibility and the catalytic activity cannot be unambiguously concluded. However, a general trend can be derived from the TPR measurements: i) Silica and titania supported catalysts reduce at low temperatures, followed by ZSM-5 supported catalysts and finally alumina supported catalysts, ii) the reduction features shift towards higher temperatures with increasing calcination temperature.

Overall, two main trends are apparent: i) the catalysts with high catalytic activity show evidence for reduced IrOx species, increased Ir-O bond lengths and lower reduction temperatures. This trend is governed by the nature of the support and follows the trend of the Lewis acidity of the support:

$$Al_2O_3 < TiO_2 < SiO_2$$

as proposed by Yazawa et al. and Nauert et al. [26], [27], ii) increasing calcination temperatures result in increased particle sizes, bulk like IrO_2 formation, stronger Ir-O bonds and higher reduction temperatures. The catalytic activity for total oxidation of propane slightly decreases with increasing calcination temperatures and increasing particle sizes. With increasing particle size, the particle becomes more bulk like and the inductive influence (-I effect) of the acidic support is expected to decrease. Therefore, the decreasing activity with increasing calcination temperature might be a result of the reduced interaction with the acidic support. Our findings are summarized in Scheme 1 on the left hand side. On the right hand side of Scheme 1 a possible reaction path following a Mars-van-Krevelen mechanism is schematically presented, highlighting the importance of the reducibility of the IrOx catalyst for the total oxidation of VOCs. We note, that a mechanistic investigation of the reaction is not part of this article and further investigations will be necessary to reveal the reaction pathway for alkane.

Therefore, the higher reactivity observed in Ir-catalysts can be ascribed to highly reducible Ir species with weakened Ir-O bonds. This effect is similar to that observed in some cases for Pt catalysts. However, for platinum catalysts the size of the platinum nanoparticles seems to determine the Pt-O bond strength [52] in the case of iridium catalysts the nature of the support is the main factor that controls the interaction, with the particle size only exerting a minor influence.
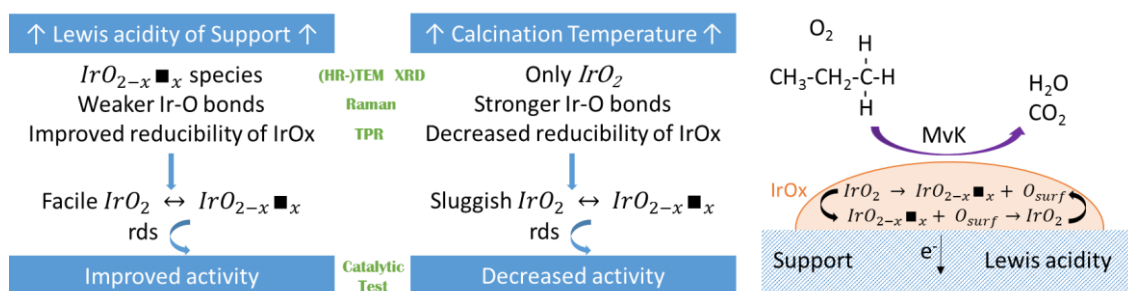
Scheme 1: The most important findings are summarized together with a possible explanation on the left hand side. A possible reaction path following a Mars-van-Krevelen mechanism (MvK) is schematically presented on the right hand side.

Conclusions

Supported iridium catalysts show high activity for the total oxidation of alkanes if the support is appropriately selected. Silica, ZSM-5 and titania are suitable supports for iridium, whereas alumina has been shown to be the least efficient.

The intrinsic catalytic activity of the IrO_2 correlates well with the Lewis acidity of the support – the higher the Lewis acidity of the support, the higher the turnover frequency of the IrOx catalyst. Physicochemical characterization of the supported IrOx shows evidence for weaker Ir-O bonds and a few metallic Ir sites in the most active catalysts. Initial deactivation of the most active catalysts most likely originates from the exhaustion of these non-oxidised species.

With increasing calcination temperatures the particle size of the IrOx catalyst increases, the reducibility of IrO_2 decreases and the strength of Ir-O bonds become slightly stronger. The decreased activity of the catalyst calcined at high temperatures exceeds the pure influence of the surface area (see decreased TOF with increasing calcination temperature). This effect is ascribed to a decreased impact of the Lewis acidity on more bulk like particles when calcined at higher temperature. Contrary to PtOx and PdOx

catalysts, the influence of the Lewis acidity of the support exceeds the influence of the particle size on the activity of IrOx catalysts for the total oxidation of short chain alkanes.

We believe that these results provide a valuable guideline for the future development of highly active supported IrOx catalysts for the total oxidation of VOCs.

References

[1] B. McDonald, J. de Gouw, J. Gilman, S. Jathar, A. Akherati, C. Cappa, J. Jimenez, J. Lee-Taylor, P. Hayes, S. McKeen, Y. Cui, S. Kim, D. Gentner, G. Isaacman-VanWertz, A. Goldstein, R. Harley, G. Frost, J. Roberts, T. Ryerson, M. Trainer, Volatile chemical products emerging as largest petrochemical source of urban organic emissions, Sci. 359 (2018) 760-764.

[2] H. Huang, Y. Xu, Q. Feng, D. Y. C. Leung, Low temperature catalytic oxidation of volatile organic compounds: a review, Catal. Sci. Technol. 5 (2015) 2649-2669.

[3] T. Garcia, B. Solsona, H. Taylor, The catalytic oxidation of hydrocarbon volatile organic compounds, Handbook of advanced methods and processes in oxidation catalysis: From laboratory to industry, (2011) 51-90.

[4] A. Berenjian, N. Chan, H. J. Malmiri, Volatile organic compounds removal methods: A review, Am. J. Biochem. Biotechnol. 8 (2012) 220–229.

[5] K. W. Shah, W. Li, A review on catalytic nanomaterials for volatile organic compounds VOC removal and their applications for healthy buildings, Nanomater. 9 (2019) 910.

[6] H. Ohtsuka, The oxidation of methane at low temperatures over zirconia-supported Pd, Ir and Pt catalysts and deactivation by sulfur poisoning, Catal. Letters. 141 (2011) 413–419.

[7] V. P. Santos, S. A. C. Carabineiro, P. B. Tavares, M. F. R. Pereira, J. J. M. Órfão, J. L. Figueiredo, Oxidation of CO, ethanol and toluene over TiO_2 supported noble metal catalysts, Appl. Catal. B Environ. 99 (2010) 198–205.

[8] X. Sun, J. Lin, Y. Wang, L. Li, X. Pan, Y. Su, X. Wang, Catalytically active Ir0 species supported on Al2O3 for complete oxidation of formaldehyde at ambient temperature, Appl. Catal. B Environ. 268 (2020) 118741.

[9] L. Schick, R. Sanchis, V. González-Alfaro, S. Agouram, J.M. López, L. Torrente-Murciano, T. García, B. Solsona, Size-activity relationship of iridium particles supported on silica for the total oxidation of volatile organic compounds (VOCs), Chem. Eng. J. 366 (2019) 100-111.

[10] Y. Lu, J. Wang, L. Yu, L. Kovarik, X. Zhang, A. Hoffman, A. Gallo, S. Bare, D. Sokaras, T. Kroll, V. Dagle, H. Xin, A. Karim, Identification of the active complex for CO oxidation over single-atom Ir-on-MgAl2O4 catalysts, Nat. Catal. 2 (2018) 149-156.

[11] J. Lin, A. Wang, B. Qiao, X. Liu, X. Yang, X. Wang, J. Liang, J. Li, J. Liu, T. Zhang, Remarkable performance of Ir1/FeOx single-atom catalyst in water gas shift reaction, J. Am. Chem. Soc. 135 (2013) 15314–15317.

[12] J. Ternel, J. L. Couturier, J. L. Dubois, J. F. Carpentier, Rhodium versus iridium catalysts in the controlled tandem hydroformylation-isomerization of functionalized unsaturated fatty substrates, Chem. Cat. Chem. 7 (2015) 513–520.

[13] D. A. Petrone, M. Isomura, I. Franzoni, S. L. Rössler, E. M. Carreira, Allenylic carbonates in enantioselective iridium-catalyzed alkylations, J. Am. Chem. Soc. 140 (2018) 4697–4704.

[14] A. Haas, S. Rabl, M. Ferrari, V. Calemma, J. Weitkamp, Ring opening of decalin via hydrogenolysis on Ir/- and Pt/silica catalysts, Appl. Catal. A Gen. 425 (2012) 97-109.

[15] J. Liu, S. Krajangsri, J. Yang, J.-Q. Li, P. G. Andersson, Iridium-catalysed asymmetric hydrogenation of allylic alcohols via dynamic kinetic resolution, Nat. Catal. 1 (2018) 438–443.

[16] G. C. da Silva, M. R. Fernandes, E. A. Ticianelli, Activity and stability of Pt/IrO2 bifunctional materials as catalysts for the oxygen evolution/reduction reactions, ACS Catal. 8 (2018) 2081–2092.

[17] C. Zhang, Q. Lai, J. H. Holles, Ir@Pt bimetallic overlayer catalysts for aqueous phase glycerol hydrodeoxygenation, Appl. Catal. A. Gen. 526 (2016) 113–125.

[18] A. H. Pizarro, C. B. Molina, J. L. G. Fierro, J. J. Rodriguez, On the effect of Ce incorporation on pillared clay-supported Pt and Ir catalysts for aqueous-phase hydrodechlorination, Appl. Catal. B Environ. 197 (2016) 236–243.

[19] A. J. Pamphile-Adrián, P. P. Florez-Rodriguez, M. H. M. Pires, G. Perez, F. B. Passos, Selective hydrogenolysis of glycerol over Ir-Ni bimetallic catalysts, Catal. Today. 289 (2017) 302–308.

[20] I.L. Shabalin, Carbon (graphene/graphite). Ultra-high temperature materials I. Springer, Dordrecht, (2014) 7-235.

[21] D. B. Rogers, R. D. Shannon, A. W. Sleight, J. L. Gillson, Crystal chemistry of metal dioxides with rutile-related structures, Inorg. Chem. 8 (1969) 841–849.

[22] Y. B. He, A. Stierle, W. X. Li, A. Farkas, N. Kasper, H. Over, Oxidation of Ir(111): From O-Ir-O trilayer to bulk oxide formation, J. Phys. Chem. C. 112 (2008) 11946–11953.

[23] G. Brauer, Handbook of Preparative Inorganic Chemistry, 2. Elsevier, 2012.

[24] P. Reyes, M. Aguirre, G. Pecchi, J.L.G. Fierro, Crotonaldehyde hydrogenation on Rh supported catalysts. Boletín de la Sociedad Chilena de Química, 45 (2000) 155-164.

[25] Y. Yazawa, H. Yoshida, S. I. Komai, T. Hattori, The additive effect on propane combustion over platinum catalyst: Control of the oxidation-resistance of platinum by the electronegativity of additives, Appl. Catal. A Gen. 233 (2002) 113–124.

[26] Y. Yazawa, H. Yoshida, S. I. Komai, T. Hattori, The additive effect on propane combustion over platinum catalyst: Control of the oxidation-resistance of platinum by the acid strength of support materials, Appl. Catal. A Gen. 233 (2002) 103–112.

[27] S. L. Nauert, L. Savereide, J. M. Notestein, Role of support lewis acid strength in copper-oxide-catalyzed oxidative dehydrogenation of cyclohexane, ACS Catal. 8 (2018) 7598–7607.

[28] S. K. Cheah, L. Massin, M. Aouine, M. C. Steil, J. Fouletier, P. Gélin, Methane steam reforming in water deficient conditions on Ir/Ce0.9Gd0.1O2-x catalyst: Metal-support interactions and catalytic activity enhancement, Appl. Catal. B Environ. 234 (2018) 279–289.

[29] F. Huang, Y. Deng, Y. Chen, X. Cai, M. Peng, Z. Jia, J. Xie, D. Xiao, X. Wen, N. Wang, Z. Jiang, H. Liu, D. Ma, Anchoring Cu 1 species over nanodiamond-graphene for semi-hydrogenation of acetylene, Nat. Commun. 10 (2019) 1-7.

[30] J. Zhang, Y. Deng, X. Cai, Y. Chen, M. Peng, Z. Jia, Z. Jiang, P. Ren, S. Yao, J. Xie, D. Xiao, X. Wen, N. Wang, H. Liu, D. Ma, Tin-assisted fully exposed platinum clusters

stabilized on defect-rich graphene for dehydrogenation reaction, ACS Catal. 9 (2019) 5998-6005.

[31] L. Xia, D. Li, J. Long, F. Huang, L. Yang, Y. Guo, Z. Jia, J. Xiao, H. Liu, N-doped graphene confined Pt nanoparticles for efficient semi-hydrogenation of phenylacetylene, Carbon. 145 (2019) 47-52.

[32] T. R. Baldwin, R. Burch, Catalytic combustion of methane over supported palladium catalysts: I. Alumina supported catalysts, Appl. Catal. 66 (1990) 337–358.

[33] T. V. Choudhary, S. Banerjee, V. R. Choudhary, Catalysts for combustion of methane and lower alkanes, Appl. Catal. A Gen. 234 (2002) 1–23.

[34] R. F. Hicks, H. Qi, M. L. Young, R. G. Lee, Structure sensitivity of methane oxidation over platinum and palladium, J. Catal. 122 (1990) 280–294.

[35] K. I. Fujimoto, F. H. Ribeiro, M. Avalos-Borja, E. Iglesia, Structure and reactivity of PdOx/ZrO2 catalysts for methane oxidation at low temperatures, J. Catal. 179 (1998) 431–442.

[36] L. Torrente-Murciano, B. Solsona, S. Agouram, R. Sanchis, J.M. López, T. García, R. Zanella, Low temperature total oxidation of toluene by bimetallic Au-Ir catalysts, Catal. Sci. Technol. 7 (2017) 2886–2896.

[37] T. Maillet, C. Solleau, J. Barbier, D. Duprez, Oxidation of carbon monoxide, propene, propane and methane over a Pd/Al2O3 catalyst. Effect of the chemical state of Pd, Appl. Catal. B Environ. 14 (1997) 85–95.

[38] G. I. B. T.-S. in S. S. and C. Golodets, Ed., "Chapter XV: The Oxidation of Paraffins," in Heterogeneous Catalytic Reactions Involving Molecular Oxygen, Elsevier 15 (1983) Elsevier, 437–469.

[39] H. A. Wriedt, The Al-O (aluminum-oxygen) system. Bulletin of Alloy Phase Diagrams 6 (1985) 548-553.

[40] T. Tsukada, H. Segawa, A. Yasumori, K. Okada, Crystallinity of boehmite and its effect on the phase transition, J. Mater. Chem. 9 (1999) 549–553.

[41] B. J. L. Murray, H. A. Wriedt, The O-Ti (oxygen-titanium) system, Bulletin of Alloy Phase Diagrams, 8 (1987) 148–165.

[42] L. Torrente-Murciano, The importance of particle-support interaction on particle size determination by gas chemisorption, J. Nanopart. Res. 18 (2016) 1–7.

[43] S. Krishnamurthy, G. R. Landolt, H. J. Schoennagel, The stoichiometry of hydrogen and CO chemisorption on Irγ-Al2O3, J. Catal. 78 (1982) 319–326

[44] T.I. Koranyi, J. Mihaly, E. Pfeifer, C. Nemeth, T. Yuzhakova, J. Mink, Infrared Emission and Theoretical Study of Carbon Monoxide Adsorbed on Alumina-Supported Rh, Ir, and Pt Catalysts J. Phys. Chem. A 110 (2006) 1817-1823.

[45] G. B. McVicker, R. T. K. Baker, R. L. Garten, E. L. Kugler, Chemisorption properties of iridium on alumina catalysts, J. Catal. 65 (1980) 207–220.

[46] B. J. Kip, F. B. M. Duivenvoorden, D. C. Koningsberger, R. Prins, Determination of metal particle size of highly dispersed Rh, Ir, and Pt catalysts by hydrogen chemisorption and EXAFS, J. Catal. 105 (1987) 26–38.

[47] S. J. Freakley, J. Ruiz-Esquius, D. J. Morgan, The X-ray photoelectron spectra of Ir, IrO2 and IrCl3 revisited, Surf. Interface Anal. 49 (2017) 794–799.

[48] Y. S. Huang, S. S. Lin, C. R. Huang, M. C. Lee, T. E. Dann, F. Z. Chien, Raman spectrum of IrO2, Solid State Commun. 70 (1989) 517–522.

[49] S. E. Deutsch, J. T. Miller, K. Tomishige, Y. Iwasawa, W. A. Weber, B. C. Gates, Supported Ir and Pt clusters: Reactivity with oxygen investigated by extended X-ray absorption fine structure spectroscopy, J. Phys. Chem. 100 (1996) 13408–13415.

[50] W. Banerjee, S. Maikap, T. C. Tien, W. C. Li, J. R. Yang, Impact of metal nano layer thickness on tunneling oxide and memory performance of core-shell iridium-oxide nanocrystals, J. Appl. Phys. 110 (2011) 074309.

[51] R. Jin, M. Peng, A. Li, Y. Deng, Z. Jia, F. Huang, Y. Ling, F. Yang, H. Fu, J. Xie, X. Han, D. Xiao, Z. Jiang, H. Liu, D. Ma, Low temperature oxidation of ethane to oxygenates by oxygen over iridium-cluster catalysts, J. Am. Chem. Soc. 141 (2019) 18921–18925.

[52] H. Huang, P. Hu, H. Huang, J. Chen, X. Ye, D. Y. C. Leung, Highly dispersed and active supported Pt nanoparticles for gaseous formaldehyde oxidation: Influence of particle size, Chem. Eng. J. 252 (2014) 320–326.